



HAL
open science

Conditional existence of Donnan potential in soft particles and surfaces: Dependence on steric effects mediated by electrolyte ions and structural charges

Nicolas Lesniewska, Audrey Beaussart, Jérôme F.L. Duval

► **To cite this version:**

Nicolas Lesniewska, Audrey Beaussart, Jérôme F.L. Duval. Conditional existence of Donnan potential in soft particles and surfaces: Dependence on steric effects mediated by electrolyte ions and structural charges. *Journal of Molecular Liquids*, 2023, 387, pp.122643. 10.1016/j.molliq.2023.122643 . hal-04175760

HAL Id: hal-04175760

<https://hal.univ-lorraine.fr/hal-04175760>

Submitted on 24 Oct 2023

HAL is a multi-disciplinary open access archive for the deposit and dissemination of scientific research documents, whether they are published or not. The documents may come from teaching and research institutions in France or abroad, or from public or private research centers.

L'archive ouverte pluridisciplinaire **HAL**, est destinée au dépôt et à la diffusion de documents scientifiques de niveau recherche, publiés ou non, émanant des établissements d'enseignement et de recherche français ou étrangers, des laboratoires publics ou privés.

Public Domain

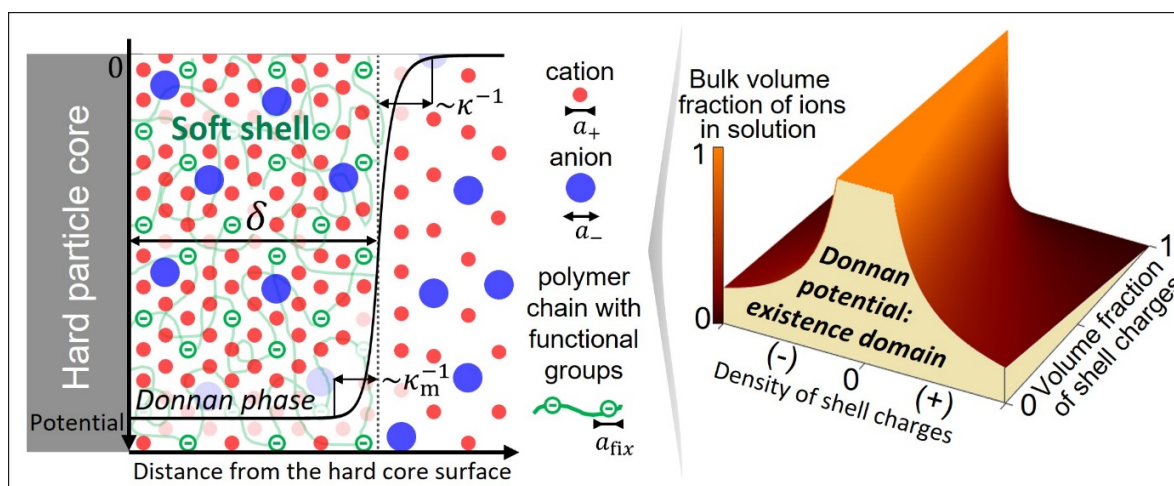
1 **Conditional existence of Donnan potential in soft particles and surfaces: dependence on**
2 **steric effects mediated by electrolyte ions and structural charges.**

3
4 Nicolas Lesniewska*, Audrey Beaussart, Jérôme F.L. Duval*

5 Université de Lorraine, CNRS, Laboratoire Interdisciplinaire des Environnements Continentaux (LIEC),
6 UMR 7360, Vandoeuvre-lès-Nancy F-54500, France

7 *Corresponding authors: nicolas.lesniewska@univ-lorraine.fr, jerome.duval@univ-lorraine.fr

8
9 **Graphical Abstract**
10



11

12 **Abstract.**

13 When a charged layer decorating a particle or a macroscopic surface is equilibrated with an electrolyte
14 solution, a constant Donnan potential is established through that layer due to charge-driven accumulation
15 of counterions and companion exclusion of coions. This situation arises when the thickness of the surface
16 layer well exceeds the screening Debye length, a condition derived from mean-field Poisson-Boltzmann
17 theory within point-like charge approximation. Herein, we revisit this condition underlying the
18 applicability of Donnan electrostatic representation with the account of steric effects mediated by the
19 sizes of the electrolyte ions and structural layer charges. A transcendental equation is derived for the
20 Donnan potential as a function of sizes and valences of anions and cations, electrolyte concentration and
21 size of the layer charges, and a closed-form expression is provided for symmetrical electrolytes. Therefrom
22 we evidence that the existence of a Donnan potential is conditioned not only to large values of the layer
23 thickness compared to a here-defined Debye length operative within the shell, but to additional
24 verification of a criterion that involves space charge density of the layer, solution ionic strength and
25 electrolyte nondiluteness parameter. Illustrative computational examples show how the existence and
26 magnitude of the Donnan potential depend on the key molecular descriptors of the electrolyte and soft
27 interface, and they further quantify the deviations from predictions based on classical Donnan potential
28 expression valid for dilute electrolytes.

29
30
31
32
33
34
35
36
37
38

39 **Keywords:** Soft particles/interfaces, Electrostatics, Donnan potential, Steric effects, Modified Poisson-
40 Boltzmann theory

41

42 **1. Introduction.**

43 Electrostatics plays a key role in the reactivity of particles and (bio)interfaces, e.g. colloid stability [1],
44 ion adsorption [2], electrokinetics [3], polyelectrolyte swelling [4], cell biology [5-7], or blue energy
45 harvesting [8]. Accordingly, modelling the electrostatics of charged interfaces and particles is of
46 paramount importance, and formalisms reported for that purpose include the well-known mean-field
47 Poisson-Boltzmann (PB) theory [9] and extensions thereof [10-22], and advanced molecular simulations
48 [2,23-27]. Electrostatics of so-called soft colloids, i.e. colloids that consist partly or entirely of ion-
49 permeable polyelectrolyte-like material with 3D distributed structural charges (e.g. microbial surfaces,
50 viruses, engineered particle surface coatings, natural organic matter, macromolecules) [3,28-32], has
51 received much attention by the community due to the ubiquity of these colloidal systems in biological and
52 environmental settings [31,32], and their use in applications as diverse as drug delivery [33], degradation
53 of organic pollutants [34], water treatment [35] or control of pathogens biofilm formation [36].

54 Following the pioneering work by Ohshima on soft surface electrostatics (cf. [3,29] and references
55 therein), the equilibrium potential distribution at the interface formed between an electrolyte solution
56 and a hard (ion-impermeable) core-soft shell particle, a porous particle (i.e. devoid of core) or a
57 polyelectrolyte-coated planar surface has been derived from numerical and analytical solutions of PB
58 equation with account of the charge contributions from both the electrolyte ions and the functional
59 groups distributed within the shell material [29-32,37-40]. Solutions of PB equation have been further
60 reported for soft particles in homo- or hetero-electrostatic interaction configurations [41-43] and for
61 heterogeneous soft surface layers defined by a density of structural charges that varies with space [39,44].
62 A case of practical interest naturally emerges from the PB equation written for a soft surface layer whose
63 thickness exceeds significantly the screening Debye length (hereafter denoted as $1/\kappa$): this is the Donnan
64 situation where the electrostatic potential is constant inside the charged layer and decays to zero value
65 over distances of the order $1/\kappa$ on both sides of the soft layer/electrolyte solution interface [45-48].
66 Under such a condition, Ohshima [45] demonstrated the equivalence between PB-derived expression of
67 the interfacial potential drop – the so-called Donnan potential – and the one reported earlier by assuming
68 simple local electroneutrality within the layer [49,50]. Remarkably, it is only recently that a direct support
69 of Donnan potential theory was evidenced by tender-ambient pressure X-ray photoelectron spectroscopy
70 measurements on ion-exchange membranes equilibrated with electrolyte solutions [51], while earlier
71 indirect measurements have been reported on charged hydrogels by in-situ microelectrode voltammetry
72 [52]. The Donnan partitioning of ions at charged surfaces and permselective interfaces has major
73 implications in biology, as e.g. it affects the permeability of the membrane of Gram-negative bacteria to

74 nutrients or antibiotics [7], it contributes to bacterial survival under adverse (osmotic) environments [53]
75 and it connects to biological functions like electric signalling in nervous system [54].

76 Whereas Donnan potential is achieved in charged surface layers at sufficiently high salt concentrations
77 where the condition of thin electric double layer (EDL) compared to soft surface layer thickness is met,
78 the combined effects of ion size *and* size of layer charges on interfacial Donnan partitioning of ions have
79 – to the best of our knowledge – received little attention, despite the expected increase of the
80 contributions of such effects with increasing electrolyte concentration [55-57]. A modification of the
81 mean-field PB equation for soft interfaces and corresponding derivation of Donnan potential expression,
82 have been reported so far for the only restrictive case of symmetrical electrolytes where anions and
83 cations are assumed to have similar size, and considering layer charges as point-like [58-60]. Under these
84 conditions, Lesniewska et al. [60] further derived an expression underlying the applicability of the Donnan
85 representation for soft surface layer electrostatics as a function of the nondiluteness of the electrolyte,
86 thereby evidencing that the condition of a sufficiently thin electric double layer is not sufficient to warrant
87 the development of a Donnan potential in a charged soft surface layer.

88 Here, we further elaborate on this latest development and report an original expression for the Donnan
89 potential in the most generic situation where anions and cations are defined by dissimilar valences and
90 sizes, and where the size of charges carried by the soft surface layer is considered explicitly. This extension
91 calls for the exploitation of an involved expression for the mixture entropy of the {layer charges/ions}
92 system and of the corresponding PB formulation, as derived recently by Lesniewska et al. [60]. In turn, the
93 formalism leads to a rationale of the situations where a Donnan potential cannot develop in the surface
94 layer, even at high salt concentrations, due to limitation in the neutralization of layer charges by ions as a
95 result of excluded volumes of anions, cations and functional groups carried by the layer. Illustrative
96 computations further quantify the effects of electrolyte concentration, size/valence of ions and layer
97 charges on *both* the existence domain and magnitude of the Donnan potential, while evidencing the
98 moderate to severe misevaluation of the Donnan potential by predictions applicable to dilute systems
99 where steric effects are discarded. Among the important results provided in this work is the derivation of
100 the expression for the thickness of the electric double layer operative inside the charged surface layer, as
101 a function of the ions- and shell charges- properties that govern steric effects.

102

103 **2. Theory.**

104 2.1. Electrostatics of soft interfaces.

105 In this section, we recall the basics of the electrostatic formalism recently developed by Lesniewska et
106 al. [60] for soft interfaces in aqueous media. We elaborate below on this formalism with the objective to
107 formulate explicitly the conditions underlying the existence of a Donnan potential in a given shell layer
108 depending on the nondiluteness of the electrolyte. Herein, we consider a spherical core-shell particle with
109 radius $r_p = r_c + \delta$, where r_c (m) and δ (m) are the particle core radius and shell layer thickness,
110 respectively (**Figure 1**). The developments below hold in the electric double layer regime $\kappa r_p \gg 1$ where
111 $1/\kappa$ (m) is the Debye layer thickness defined by $1/\kappa = 1/\sqrt{2F^2 I / (RT \epsilon_0 \epsilon_s)}$ with ϵ_0 the dielectric
112 permittivity of the vacuum, ϵ_s the relative dielectric permittivity of the aqueous medium, R the gas
113 constant, T the absolute temperature, F the Faraday number, and I (mol m⁻³) the solution ionic
114 strength. Adopting a radial coordinate system where $r=0$ refers to the centre of the particle, we
115 introduce for convenience the dimensionless radial position X defined by $X = \kappa(r - r_c)$. In the following,
116 we further consider an electrolyte solution with cations and anions of *unsigned valences* z_+ and z_- , and
117 *effective radii* a_+ (m) and a_- (m), respectively, with a_+^3 and a_-^3 their volumes assumed incompressible.
118 The (number) densities of the cations and anions at radial position r are denoted as $c_{+,-}(r)$ (m⁻³), and
119 their bulk concentrations are defined by $c_{+,-}(r \rightarrow \infty) = c_{+,-}^\infty$ with the electroneutrality condition given by
120 $z_+ c_+^\infty - z_- c_-^\infty = 0$ (autoprotolysis of water is neglected). The latter condition is systematically verified upon
121 introduction of the number density c_0 (m⁻³) defined by $c_0 = c_+^\infty / z_+ = c_-^\infty / z_-$. In turn, solution ionic strength
122 I is provided by $I = z_+ z_- (z_+ + z_-) c_0 / (2N_A)$ where N_A is the Avogadro number.

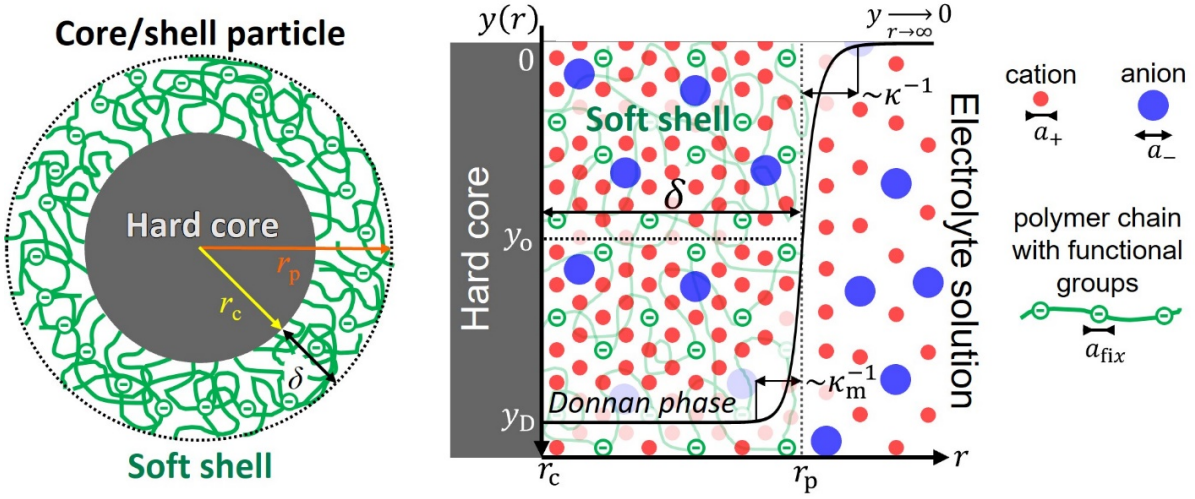


Figure 1. (Left) Schematic representation of a core-polyelectrolyte shell particle where the nomenclature adopted for the radial coordinate system (r), the particle core radius (r_c) and the shell thickness (δ) is specified. (Right) Zoom of the core/shell/aqueous electrolyte interfaces for cases where a Donnan potential is achieved in the particle shell layer. In the current work, the finite size of cations and anions ($a_{+,-}$) and that of the shell charges (a_{fix}) carried by the polymer chains constituting the shell layer are considered for the formulation of the electrostatic potential distribution within and outside the shell layer. In the shown example, the surface of the particle core is uncharged so that the electric field at $r = r_c$ is zero, and the particle shell is negatively charged. The purpose of the work is to formulate explicitly the conditions validating such a Donnan electrostatic situation depending on the geometric descriptors of the particle, the nondiluteness of the electrolyte, the excluded volume and density of the charges distributed within the shell component of the core-shell particle. $1/\kappa_m$ and $1/\kappa$ refer to the thickness of the screening Debye layers operative in the shell medium and in the outer electrolyte solution, respectively. $y(r)$, y_0 and y_D correspond to the (dimensionless) potential at position r , the potential at the outer surface of the shell layer and the Donnan potential, respectively. Cf. details in the text.

123

124 In the developments below, we denote as a_{fix} (m) the radius of the structural charges (incompressible
 125 volume a_{fix}^3) distributed within the particle shell layer. To ease developments, and in line with common
 126 assumptions [3,29,42,43], the distribution of the structural charges within the shell is considered
 127 homogeneous so that the shell charge density denoted as $\rho_{fix}(r)$ ($C\ m^{-3}$) is given by

$$128 \quad \rho_{fix}(r) = \begin{cases} \rho_0 & \text{for } r_c \leq r \leq r_p \\ 0 & \text{for } r > r_p \end{cases} \quad (1)$$

129 where $|\rho_0| = Zec_{fix,0}$ is the density of shell charges with unsigned valence Z and number density $c_{fix,0}$ (m^{-3}), and e is the elementary charge. Similarly, we introduce $c_{fix}(r) = |\rho_{fix}(r)|/(Ze)$ (m^{-3}) the number
 130 density of shell charges at position r . In the electric double layer regime defined by $\kappa r_p \gg 1$, the mean-
 131

132 field Poisson-Boltzmann equation applicable to soft interfaces (termed **SMFPB** equation) and modified to
 133 account for the steric effects mediated by the size of the electrolyte ions and shell charges, reads [60]

$$134 \quad \frac{d^2 y(X)}{dX^2} = \frac{n_-(X) - n_+(X)}{z_+ + z_-} - \frac{\rho_{\text{fix}}(X)}{2IF} \quad (2)$$

135 where $\psi(r)$ (V) is the electrostatic potential at position r and $y(r) = F\psi(r)/RT$ is the dimensionless
 136 potential. Within the framework of this study, Eq. (2) does not involve the terms formulated by Lesniewska
 137 et al. [60] that originate from ion-ion correlations and dielectric decrement effect because their respective
 138 contributions were shown to be irrelevant for the cases of interest here where Donnan electrostatic
 139 representation is applicable [60]. The quantities $n_+(r) = c_+(r)/c_+^\infty$ and $n_-(r) = c_-(r)/c_-^\infty$ in Eq. (2)
 140 correspond to the (dimensionless) concentrations of cations and anions at position r , respectively.
 141 Discarding ion-ion correlations and dielectric effect, $n_{\pm}(r)$ are defined by (for $a_+ \geq a_-$)

$$142 \quad \begin{cases} n_+(r) = \frac{e^{-z_+ y(r)}}{g_{\text{cc}}(y(r))} & \text{(a)} \\ n_-(r) = \frac{f_{\text{cc}}(y(r)) e^{z_- y(r)}}{g_{\text{cc}}(y(r))} & \text{(b)} \end{cases} \quad (3)$$

143 where f_{cc} and g_{cc} are functions of the potential distribution $y(r)$ defined by

$$144 \quad \begin{cases} f_{\text{cc}}(y(r)) = \left(\frac{1 - \nu + a_-^3 c_0 z_+ e^{z_- y(r)}}{1 - a_+^3 c_0 z_-} \right)^{(a_+/a_-)^3 - 1} & \text{(a)} \\ g_{\text{cc}}(y(r)) = \frac{f_{\text{cc}}(y(r))(1 - \nu) + a_+^3 c_0 z_- e^{-z_+ y(r)} + a_-^3 c_0 z_+ f_{\text{cc}}(y(r)) e^{z_- y(r)}}{1 - a_{\text{fix}}^3 c_{\text{fix}}(r)} & \text{(b)} \end{cases} \quad (4)$$

145 with $\nu = \sum_{\text{ion } i} a_i^3 c_i^\infty (< 1)$ a measure of the nondiluteness of the electrolyte. This definition of ν , adopted
 146 here for a convenient formulation of the Donnan electrostatic potential (cf. developments below), differs
 147 from the one adopted in [60] and originally defined on the basis of geometric arguments by Kilic et al.
 148 [61]. Eqs. (3)-(4) hold for $a_+ \geq a_-$, and equivalent formulation for $a_- \geq a_+$ is obtained by interchanging the
 149 terms $e^{z_- y}$ and $e^{-z_+ y}$ and the subscripts '+' and '-' in Eqs. (3)-(4). In Eq. (4), the function $g_{\text{cc}}(y(r))$ accounts
 150 for the decrease in ion concentrations at position r due to excluded volume effects, as compared to the
 151 common mean-field situation where ions and shell charges are point-like [21,60]. In addition, $f_{\text{cc}}(y(r))$
 152 in Eq. (4) reflects the way in which an asymmetry in anion and cation sizes impacts on the potential
 153 distribution $y(r)$, with the limit $f_{\text{cc}}(y(r)) = 1$ achieved for $a_+ = a_-$.

154

155 2.2. Donnan potential: the classical picture of point-like charges.

156 For core-shell particles featuring a shell density distribution given by Eq. (1), the Donnan phase (when
157 existing) corresponds to the shell region where the electrostatic field is zero (**Figure 1**). This situation is
158 achieved for soft particulate (and planar) interfaces whose shell dimension well exceeds the thickness of
159 the electrical double layer thickness $1/\kappa$. The corresponding condition $\kappa\delta \gg 1$ thus applies to sufficiently
160 thick shell layers and/or sufficiently high electrolyte concentrations [45]. Under such conditions, Ohshima
161 formulated the potential distribution within the shell layer and at the shell solution interface [62]. He
162 evidenced that the Debye layer thickness operative at the shell side of the interface, denoted as $1/\kappa_m$
163 (m), generally differs from the conventional Debye screening length $1/\kappa$ according to

$$164 \quad 1/\kappa_m = 1/\left(\kappa\sqrt{\cosh(zy_D)}\right) \quad (5)$$

165 which is valid for a symmetric $z:z$ electrolyte, with $y_D = F\psi_D/RT$ the dimensionless Donnan potential
166 defined by $y_D = z^{-1}\text{asinh}(z\rho_0/(2IF))$ reached in the bulk shell layer (**Figure 1**) and asinh corresponds to
167 the inverse hyperbolic sine function. The length scale $1/\kappa_m$ basically refers to the distance over which the
168 potential (in absolute value) decreases from $|y_D|$ to the potential value at the interface formed with the
169 outer electrolyte solution (i.e. at $r=r_p$), as schemed in **Figure 1**. Eq. (5) highlights that the electrostatic
170 potential distribution at the shell and water sides of the shell/solution interface becomes asymmetric for
171 sufficiently charged soft systems, as $1/\kappa_m$ differs from $1/\kappa$ with increasing the magnitude of the Donnan
172 potential, and a similar conclusion holds with increasing electrolyte valence z . In turn, a Donnan phase is
173 actually effective within the particle shell provided that the shell thickness δ is significantly larger than
174 the intraparticulate screening distance, i.e. $\kappa_m\delta \gg 1$. As the inequality $\kappa_m \geq \kappa$ (cf. Eq. (5)) is always
175 verified, the true condition $\kappa_m\delta \gg 1$ underlying the applicability of a Donnan potential in the particle shell
176 is commonly replaced by $\kappa\delta \gg 1$, which has the merit to be independent of y_D .

177

178 2.3. Conditional existence of a Donnan potential with account of steric effects.

179 Following Lesniewska et al. [60], the steric effects governed by the excluded volumes of ions and shell
180 charges may significantly modulate the electrostatic potential distribution at soft interfaces, as compared
181 to predictions from classical mean-field PB equation where ions and shell charges are assumed to be
182 point-like. In addition, the screening of the shell charges by electrolyte ions can be either stronger or
183 weaker than that expected from standard point-like electrostatic theory, depending on the respective
184 magnitudes of the steric descriptors of the counterions, coions, and shell charges [60]. Accordingly, we

185 address below how these molecular properties of the electrolyte and shell component of the particle
 186 affect the establishment of a Donnan potential. For that purpose, we develop hereafter the expression of
 187 the electric double layer thickness that is operative within the shell (§2.3.2) so as to derive the condition
 188 that guarantees the existence of a Donnan phase within the soft layer with account of molecular steric
 189 effects. Prior to this, we formulate the additional condition required for y_D to be defined in a region
 190 where the electrostatic field is zero (§2.3.1).

191

192 *2.3.1. Impact of steric effects on the neutralization of shell charges by electrolyte counterions in a Donnan*
 193 *phase.*

194 Several reports on the electrostatics of soft interfaces provided expressions for the Donnan potential
 195 with account of steric effects mediated by electrolyte ions [58-60]. To the best of our knowledge, they are
 196 however valid only for symmetrical electrolytes and point-like structural charges. Despite of their limited
 197 applicability in e.g. complex biological media, these formulations of y_D evidence that the finite size of the
 198 ions can, in some cases, prevent the development of a Donnan potential within a given charged soft
 199 material as a result of constrained accumulation of the counterions therein, even for situations where
 200 $\kappa\delta \gg 1$. Notably, in our previous report [60] we demonstrated that the existence of a Donnan potential is
 201 tied to the verification of the inequality $1 - \nu|n_0|z > 0$ that involves the (dimensionless) density of
 202 structural charges in the shell, defined by $n_0 = \rho_0 / (2IF)$, and the bulk volume fraction of electrolyte ions,
 203 ν . In order to extend this result to more realistic cases where finite size of the shell charges may, in
 204 addition to ion steric effects, contribute to limit the accumulation of counterions in the shell, we start
 205 from the transcendental equation that governs the magnitude of the Donnan potential

206
$$n_0 = \frac{n_-(y_D) - n_+(y_D)}{(z_- + z_+)} \quad (6)$$

207 which derives from the modified soft Poisson-Boltzmann equation (**SMFPB** Eq. (2)) taken in the limit of
 208 zero-electrostatic field in the shell. The spatial condition required for such an intra-shell zero-field
 209 condition to be achieved will be specifically elaborated in §2.3.2. Then, combining Eq. (6) with Eqs. (3) and
 210 (4), it is shown after some algebra that y_D is governed by the following expression valid for symmetrical
 211 electrolytes ($a_{+,-} = a$, $z_{+,-} = z$)

212
$$y_D = z^{-1} \left[\operatorname{asinh} \left(\frac{\frac{\nu n_0 z}{1 - a_{\text{fix}}^3 c_{\text{fix},0}}}{\sqrt{1 - \left(\frac{\nu n_0 z}{1 - a_{\text{fix}}^3 c_{\text{fix},0}} \right)^2}} \right) + \operatorname{asinh} \left(\frac{\frac{(1 - \nu) n_0 z}{1 - a_{\text{fix}}^3 c_{\text{fix},0}}}{\sqrt{1 - \left(\frac{\nu n_0 z}{1 - a_{\text{fix}}^3 c_{\text{fix},0}} \right)^2}} \right) \right] \quad (7)$$

213 where the nondiluteness parameter $\nu = \sum_{\text{ion } i} a_i^3 c_i^\infty$ reduces to $\nu = 2a^3 z c_0$. It is verified that Eq. (7)

214 simplifies into $y_D|_{\nu=0} = z^{-1} \operatorname{asinh}(n_0 z)$ for $\nu = 0$, which correctly corresponds to the classical expression of

215 the Donnan potential recalled in §2 for symmetrical electrolytes with assimilating charges to immaterial

216 points in both electrolyte and shell layer ($a_{+,-} \rightarrow 0$ or, equivalently, $\nu = 0$, and $a_{\text{fix}} \rightarrow 0$, respectively)

217 [45,62]. Eq. (7) makes it transparent that y_D is properly defined provided that $1 - \nu |n_0| z / (1 - a_{\text{fix}}^3 c_{\text{fix},0})$ is

218 strictly positive, which corresponds to the generalization of our previous result $1 - \nu |n_0| z > 0$ [60] to

219 situations where the excluded volume of the structural shell charges is accounted on top of that of the

220 electrolyte ions. Adopting the 3D representation $(n_0 z ; a_{\text{fix}}^3 c_{\text{fix},0} ; \nu)$ to identify the existence domain of the

221 Donnan potential, **Figure 2** displays the envelop of equation $1 - \nu |n_0| z / (1 - a_{\text{fix}}^3 c_{\text{fix},0}) = 0$ which defines a

222 vertical asymptote for the behaviour of y_D versus $n_0 z$ at given $a_{\text{fix}}^3 c_{\text{fix},0}$ and ν (cf. Eq. (7)) : this existence

223 domain of y_D then simply corresponds to the points of coordinates $(n_0 z ; a_{\text{fix}}^3 c_{\text{fix},0} ; \nu)$ located below the

224 represented 2D envelop. As a brief recall of previous findings valid for $a_{\text{fix}} = 0$ [60], **Figure 2** shows that

225 with increasing $|n_0| z$, y_D is defined for decreasing values of ν . Stated differently, the larger is the amount

226 of structural charges in the shell, the larger is the amount of counterions required to neutralize these

227 charges and, for that very neutralization purpose, the smaller the size of the counterions must be to fit in

228 the overall volume of the shell. With the additional account of the finite size $a_{\text{fix}} > 0$ of the shell charges,

229 **Figure 2** evidences that an increase in a_{fix} lowers the maximum value of $|n_0| z$ for which y_D can be

230 achieved. In line with expectation, this constrain is most pronounced at large $|n_0| z$, i.e. for cases where

231 steric effects mediated both by electrolyte ions and shell charges most severely limit the development of

232 a Donnan potential in the shell particle component.

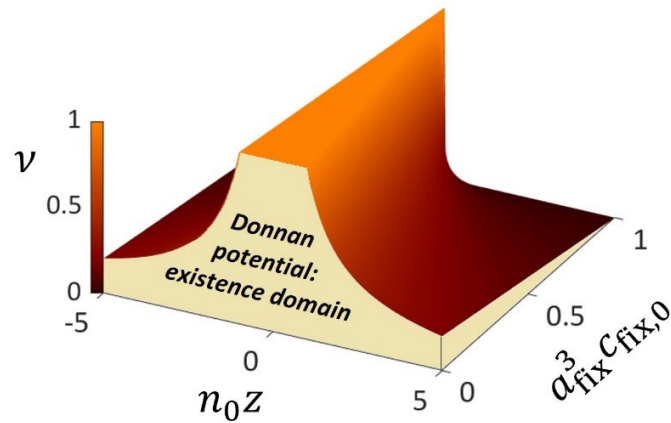


Figure 2. Existence domain of a Donnan potential for a symmetrical electrolyte containing cations and anions of similar size and valence, a and z , respectively, within the 3D representation $(n_0 z ; a_{\text{fix}}^3 c_{\text{fix},0} ; \nu)$. This existence domain (specified in the figure) is materialized by the yellow volume located under the represented envelope defined by the equation $1 - \nu |n_0| z / (1 - a_{\text{fix}}^3 c_{\text{fix},0}) = 0$, with $n_0 = \rho_0 / (2IF)$ the dimensionless charge density in the shell, $\nu = 2a^3 z c_0$ the parameter reflecting the nondiluteness of the electrolyte, and $c_{\text{fix},0} = |\rho_0| / Ze$ the number density of shell charges with effective volume a_{fix}^3 and valence Z .

233

234 For asymmetric electrolytes containing cations and anions of different valence and size, the derivation
 235 of a closed form expression for y_D is not possible and numerical solving of Eq. (3), (4) and (6) along the
 236 lines set forth in [60] is required to evaluate y_D and, therewith, identify the ranges of ion sizes and
 237 valences, and values of density and size of shell charges where y_D is defined. For such electrolytes,
 238 Lesniewska et al. [60] evidenced a similar limitation in the accumulation of ions due to steric effects (cf.
 239 **Figure 2**) with a dominant role played by the excluded volumes of the counterions. The Donnan potential
 240 will be thus evaluated in §3 as a function of n_0 , $a_{+,-}$, $z_{+,-}$ and a_{fix} using a PTC Mathcad Prime 8.0
 241 algorithm based on Levenberg-Marquardt method to solve y_D from Eqs. (3), (4) and (6). The domain of
 242 existence of y_D , as constrained by the capability of the counterions to neutralize shell charges due to
 243 their excluding volumes and that of the shell charges, will then be specified from location of the vertical
 244 asymptotes of the simulated y_D values plotted versus n_0 for prescribed values of the nondiluteness
 245 parameter, the density and size of shell structural charges. As argued for symmetrical electrolytes, this
 246 asymptote corresponds to the critical physical situation where the volume of the shell is about to be
 247 insufficient for hosting enough counterions to properly neutralize the structural charges distributed
 248 therein and, thereby, cancel the electrostatic field.

249

250 2.3.2. Condition for the establishment of a zero-electrostatic field region within the shell layer.

251 The condition for the existence of y_D as invoked in the preceding section §2.3.1 is derived with – as a
 252 starting point – the SMFPB equation modified for steric effects and taken in the limit of zero-electrostatic
 253 field in the shell material. As discussed in §2.2, this latter limit is tied to the verification of the (additional)
 254 condition that the shell layer thickness must exceed the screening Debye layer $1/\kappa_m$ that is operative in
 255 the shell material [62,63]. The expression of $1/\kappa_m$ is elaborated here for an uncharged particle core
 256 surface, i.e. $dy(r)/dr|_{r=r_c} = 0$, because there is no electrostatic contribution from the core surface to the
 257 overall potential drop at the very shell/solution interface for the Donnan situations of interest. Then,
 258 considering that the potential ‘deep’ inside the shell reaches Donnan potential value, i.e. $y(r \rightarrow r_c^+) \approx y_D$
 259 , we search for the spatial dependence of the potential distribution $\Delta y(r) = y(r) - y_D$ for positions ranging
 260 from r_c up to the outer layer surface ($r \rightarrow r_p^-$). In turn, adopting an approach similar to that used by
 261 Ohshima [62], we seek to characterise at which distance from the surface layer the potential deviates
 262 from y_D (**Figure 1**). Substituting $y(r) = \Delta y(r) + y_D$ in the modified SMFPB Eqs. (2)-(4) that define the
 263 potential and ion densities distributions, it is shown that the dependence of $\Delta y(X)$ on position for the
 264 most generic case of asymmetrical electrolytes ($a_{+,-}, z_{+,-}$) is governed – up to second order term in Δy –
 265 by the following second order differential equation

$$266 \quad d^2 \Delta y(X) / dX^2 = (\kappa_m / \kappa)^2 \Delta y(X) \quad (8)$$

267 where κ_m is defined by

$$268 \quad \kappa_m = \kappa \sqrt{\frac{(1 - a_{\text{fix}}^3 c_{\text{fix},0}) f_{\text{cc}}(y_D) \left[z_+ e^{-z_+ y_D} (\nu e^{z_+ y_D} + 1 - \nu)^2 + z_- (1 - \nu) g_{\text{cc}}(y_D) e^{z_- y_D} \right]}{(z_+ + z_-) (g_{\text{cc}}(y_D))^2 (a_-^3 c_-^\infty e^{z_- y_D} + 1 - \nu)}} \quad (9)$$

269 which is valid for $a_+ \geq a_-$. The defining expression of κ_m for cases where $a_+ \leq a_-$ is obtained by
 270 interchanging $e^{z_- y}$ and $e^{-z_+ y}$ and the subscripts ‘+’ and ‘-’ in Eq. (9). It is recalled that y_D in Eq. (9) is given
 271 by the numerical solution of Eqs. (3), (4) and (6) (cf. §2.3.1). We further verify that Eq. (9) correctly reduces
 272 to Eq. (5) applicable to point-like ions and shell charges, i.e. $a_{+,-} \rightarrow 0$, $a_{\text{fix}} \rightarrow 0$, and symmetrical
 273 electrolytes ($z_{+,-} = z$). For the sake of further comparison between situations where steric effects are and
 274 are not accounted for (cf. §3), we denote hereafter as $\kappa_{m,\text{ref}} = \kappa \sqrt{\cosh(z y_D)}$ (Eq. (5)) the reciprocal of the

275 intra-shell Debye length originally formulated by Ohshima [62] for symmetrical electrolytes and point-like
 276 charges.

277 For symmetrical electrolytes defined by $z_{+,-} = z$ and $a_{+,-} = a$, Eq. (9) simplifies into

$$278 \quad \kappa_m = \kappa \sqrt{\frac{(1 - a_{\text{fix}}^3 c_{\text{fix},0}) [(1 - \nu) \cosh(zy_D) + \nu]}{[\nu \cosh(zy_D) + (1 - \nu)]^2}} \quad (10)$$

279 where y_D is given by Eq. (7). While Eq. (7) involves the joint contributions of the nondiluteness of the
 280 electrolyte and of the excluded volume of the shell charges on y_D , Eq. (10) highlights that the Debye layer
 281 thickness within the shell, and therewith the electrostatic field at the very shell/solution, is also impacted
 282 by steric effects. For immaterial ions ($a_{+,-} \rightarrow 0$), both Eqs. (9) and (10) reduce to
 283 $\kappa_m = \kappa \sqrt{(1 - a_{\text{fix}}^3 c_{\text{fix},0}) \cosh(zy_D)}$, which pinpoints clearly that the finite excluded volume $a_{\text{fix}}^3 c_{\text{fix},0}$ of the shell
 284 charges is able to generate some asymmetry between the potential distributions at the shell and solution
 285 sides of the shell/solution interface. In addition, the presence of the term $f_{\text{cc}}(y_D)$ in Eq. (9) reveals that
 286 differentiated sizes of the counterions and coions can also contribute to the asymmetry in the potential
 287 distribution at the shell/solution interface. In the limit of highly diluted shell component ($c_{\text{fix},0} \rightarrow 0$,
 288 implying $y_D \rightarrow 0$), Eq. (9) reduces (for $a_+ \geq a_-$) to

$$289 \quad \kappa_m^{-1} \underset{c_{\text{fix},0} \rightarrow 0}{\sim} \kappa^{-1} / \sqrt{\frac{z_+ + (1 - \nu)z_-}{(z_+ + z_-)(1 - a_+^3 c_+^\infty)}} \equiv \kappa_{\text{mod}}^{-1} \quad (11)$$

290 which is nothing else than the effective Debye layer thickness operative at the electrolyte side of
 291 particle/electrolyte interface and corrected here for ions-mediated steric effects. To avoid confusion, we
 292 denote as κ_{mod}^{-1} this modified Debye length pertaining to the solution side of the particle/solution
 293 interface. Eq. (11) correctly identifies with the expression given in [60] (Eq. (13) therein). In line with
 294 expectation, we have $\kappa_{\text{mod}}^{-1} \rightarrow \kappa^{-1}$ for $\nu \rightarrow 0$ and, remarkably, this limit $\kappa_{\text{mod}}^{-1} \rightarrow \kappa^{-1}$ also applies to the
 295 situation $a_+ = a_-$. For cases where $a_+ \neq a_-$, Eq. (11) implies the inequality $\kappa_{\text{mod}}^{-1} \leq \kappa^{-1}$ (a typo mistake in [60]
 296 incorrectly indicates the reverse inequality), i.e. the screening Debye length is systematically
 297 overestimated if using the expression of κ^{-1} for situations where ion size ratio differs from unity.

298 For sake of completeness, from Eq. (8), it is straightforward to verify that the potential inside the
 299 polyelectrolyte shell can be approximated by $y(r) = y_D + (y_o - y_D) \sinh(\kappa_m(r - r_c)) / \sinh(\kappa_m \delta)$, where
 300 $y_o = y(r = r_p)$ is the potential reached at the outer layer surface. Starting from Eqs. (1)-(4) linearized for

301 low potentials $y(r) (\ll 1)$, performing a first integration of the corresponding form of Eq. (2) to evaluate
 302 the electric field at both sides of the shell/solution interface ($r = r_p^-$ and $r = r_p^+$), and finally applying the
 303 continuity condition for the potential and field at $r = r_p$, we obtain, for $a_+ \geq a_-$,

$$304 \quad y_o = y_D - \frac{y_D^2 (1 - a_{\text{fix}}^3 c_{\text{fix},0})}{2n_0} \left[\frac{z_+ + (1 - \nu) z_-}{(z_+ + z_-)(1 - a_+^3 c_+^{\infty})} \right] \equiv y_D - \frac{y_D^2 (1 - a_{\text{fix}}^3 c_{\text{fix},0})}{2n_0} \left(\frac{\kappa_{\text{mod}}}{\kappa} \right)^2 \quad (12)$$

305 where κ_{mod}^{-1} is defined by Eq. (11). Eq. (12) reduces to $y_o = y_D / 2 = n_0 / 2$ for $z_+ = z_-$, $a_{+,-} \rightarrow 0$ and $a_{\text{fix}} \rightarrow 0$
 306 , in agreement with point-like results by Ohshima applicable to z:z electrolytes [62]. Remarkably, using the
 307 relationship $y_D = n_0 (\kappa / \kappa_{\text{mod}})^2 / (1 - a_{\text{fix}}^3 c_{\text{fix},0})$ between y_D and n_0 , which is derived from Eq. (6) linearized
 308 up to first order term in y_D , Eq. (12) simplifies into $y_o = y_D / 2$ for any $a_{+,-}$, $z_{+,-}$ and a_{fix} .

309 As an intermediate conclusion, the results provided in §2.3 define the conditional existence of a
 310 Donnan potential, which is tied to the verification of two criteria: one of these criteria ensures that the
 311 required neutralization of the shell charges by counterions, necessary to achieve the Donnan potential
 312 value y_D , is not limited by the excluded volumes of the ions and shell charges (cf. §2.3.1 and **Figure 2** that
 313 illustrates the case of symmetrical electrolytes), and the other criterion $\kappa_m \delta \gg 1$, with κ_m defined by Eq.
 314 (9), relates to the needed condition for the establishment of a zero-electrostatic field region within the
 315 shell layer. In the following section, computational examples are reported for a comprehensive evaluation
 316 of both the magnitude and domain of existence of Donnan potential in the shell, depending on the valence
 317 and size of the electrolyte counterions and coions, and on the excluded volume of the structural shell
 318 charges.

319

320 **3. Results and discussion.**

321 In this section, we address the existence domain of a Donnan phase within soft surface layers for a
 322 comprehensive set of electrolyte and soft layer electrostatic settings, which includes cases of similar or
 323 differentiated cation/anion valences and sizes. For that purpose, the evolution of y_D is computed for
 324 increasing values of the structural charge density n_0 of the shell, which in turn allows the specification of
 325 the critical values of n_0 for which the congestion of ions within the shell reaches a limit due to their
 326 incompressible volumes. Given the definition $n_0 = \rho_0 / (2IF)$, we emphasize that increasing values of $|n_0|$
 327 refer to an increase in the shell charge density (in absolute value) and/or a decrease in the solution ionic
 328 strength I , while all remaining parameters ($a_{+,-}^3 c_0$, $z_{+,-}$, and $a_{\text{fix}}^3 c_{\text{fix},0}$) are kept constant. In addition, y_D

329 is systematically compared to $y_D|_{v=0}$ that refers to the standard point-like situation where $a_{+,-,\text{fix}} \rightarrow 0$. As
 330 argued in §2, a complete assessment of the existence domain of y_D further calls for the comparison of
 331 the spatial scale $1/\kappa_m$ with the shell layer thickness δ . Accordingly, for each analysed combination of
 332 ions and shell descriptors, we hereafter report the dimensionless ratio $\kappa_m^{-1}/\kappa^{-1}$ in the n_0 -interval where
 333 y_D is properly defined, the ratio $\kappa_m^{-1}/\kappa^{-1}$ offering the advantage to assess the difference between
 334 screening distance inside and outside the shell (and therewith the asymmetry of the potential distribution
 335 at the shell/solution interface). To help physical interpretation of simulations, this ratio is further
 336 compared to the ratio $\kappa_{m,\text{ref}}^{-1}/\kappa^{-1}$ (Eq. (5)) formulated by Ohshima for symmetrical electrolytes and point-
 337 like ions and shell charges.

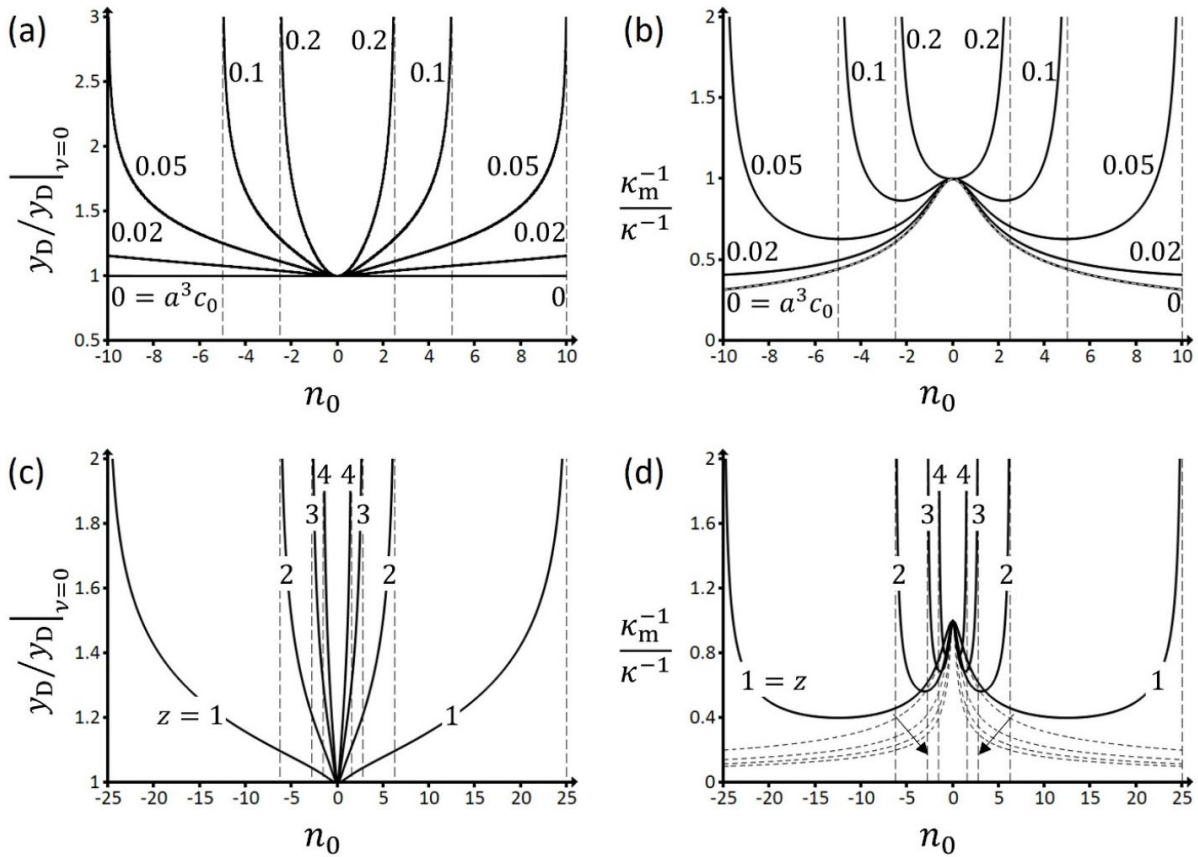


Figure 3. Donnan potential and Debye screening lengths ratios, $y_D/y_D|_{v=0}$ **(a,c)** and $\kappa_m^{-1}/\kappa^{-1}$ **(b,d)**, respectively, as a function of the dimensionless shell charge density n_0 for soft surface layers in contact with a symmetrical aqueous electrolyte defined by **(a,b)** $z_{+,-} = z=1$ and different ion volumes $a^3 c_0$ (indicated) with $a = a_{+,-}$, and **(c,d)** $a^3 c_0 = 0.02$ and different ion valences z (indicated). Results are here given with neglecting steric effects connected to the size of shell charges, i.e. $a_{\text{fix}}^3 c_{\text{fix},0} \rightarrow 0$. The dashed

curves in **(b,d)** correspond to $\kappa_{m,\text{ref}}^{-1} / \kappa^{-1}$ (Eq. (5)), and the arrows in **(d)** point to increasing values of z with $z = 1, 2, 3$ and 4 . The vertical dashed lines in all panels indicate the position $n_0 = n_0^*$ of the vertical asymptotes for $y_D / y_D|_{v=0}$ **(a,c)** and $\kappa_m^{-1} / \kappa^{-1}$ **(b,d)**. For a given set of conditions examined, these asymptotes mark the frontier n_0^* of the n_0 -domain below which a Donnan potential is defined within the shell layer, with $|n_0^*| = 1 / (\nu z)$.

338

339 **Figure 3** shows the variations of $y_D / y_D|_{v=0}$ and $\kappa_m^{-1} / \kappa^{-1}$ as a function of n_0 for symmetrical
340 electrolytes ($z_{+,-} = z$ and $a_{+,-} = a$) and, for the sake of demonstration, the steric effects due to the finite
341 size of the shell charges are here discarded ($a_{\text{fix}}^3 c_{\text{fix},0} \rightarrow 0$). For this situation, the results corresponding to
342 negatively ($n_0 < 0$) and positively ($n_0 > 0$) charged layers are symmetrical with respect to the axis $n_0 = 0$
343 , in agreement with the parity of the functions $y_D / y_D|_{v=0}$ and $\kappa_m^{-1} / \kappa^{-1}$ (Eqs. (7) and (10)). For given z
344 and a , **Figure 3a** evidences that $y_D / y_D|_{v=0}$ is larger than unity over the whole range of n_0 , and the
345 deviation of this ratio from unity increases with increasing $|n_0|$. This is so because the excluded volume of
346 the ions impairs their required accumulation in the shell for the establishment of a Donnan potential,
347 which in turn decreases the screening of the particle shell charges by the ions and increases the magnitude
348 of $y_D / y_D|_{v=0}$ (**Figure 2**). Accordingly, this increase of $y_D / y_D|_{v=0}$ becomes more important for increasing
349 values of the excluded volume of the ions at fixed value of $|n_0|$ (**Figure 3a**). The vertical asymptotes
350 appearing in the $y_D / y_D|_{v=0}$ vs. n_0 plots in **Figure 3a** are defined by the equation $n_0 = n_0^*$, with n_0^* marking
351 the frontier between the n_0 -domains where y_D is and is not defined, i.e. $|n_0| < |n_0^*|$ and $|n_0| > |n_0^*|$,
352 respectively. The value of n_0^* and, therewith, the extension of the n_0 -existence domain of y_D depends on
353 the nondiluteness of the bulk electrolyte and ion valence according to $|n_0^*| = 1 / (\nu z)$, in agreement with
354 predictions from Eq. (7) that applies to symmetrical electrolytes (cf. **Figure 2**).

355 For point-like ions (i.e. $a^3 c_0 = 0$ or, equivalently, $\nu = 0$), **Figure 3b** confirms that $\kappa_m^{-1} / \kappa^{-1}$ reduces to
356 $\kappa_{m,\text{ref}}^{-1} / \kappa^{-1}$ (Eq. (5)), which corresponds to the outcome of Ohshima's model [62]. In details, $\kappa_{m,\text{ref}}^{-1} / \kappa^{-1}$
357 decreases with $|n_0|$, in agreement with Eq. (5) that involves the Donnan potential defined, for point-like
358 ions, by $y_D|_{v=0} = z^{-1} a \sinh(n_0 z)$. This decrease in $\kappa_{m,\text{ref}}^{-1} / \kappa^{-1}$ simply features that the drop of the potential
359 from y_D to y_0 (surface potential of the shell layer defined by Eq. (12)) within the shell spans over a
360 distance shorter than that over which the potential drops in solution from y_0 to 0 (**Figure 1**). In turn, the

361 potential distribution at the shell/solution interface features a marked asymmetry as the shell gets
 362 increasingly charged or, equivalently, y_D gets higher (in absolute value). Hereafter, we denote as ' y_D -
 363 effect' this effect that underlies a pronounced asymmetry of the potential distribution at the shell/solution
 364 interface as the shell gets increasingly charged (and $|y_D|$ larger). Like $\kappa_{m,ref}^{-1} / \kappa^{-1}$, the ratio $\kappa_m^{-1} / \kappa^{-1}$
 365 decreases with $|n_0|$ for $\nu \ll 1$ (i.e. low $a^3 c_0$) and/or sufficiently low $|n_0|$ (**Figure 3b**), basically because these
 366 conditions refer to a modest accumulation of the electrolyte ions inside the shell, i.e. the contribution of
 367 the excluded volume effects on ion partitioning is not dominant. For moderate values of the excluded ion
 368 volume $a^3 c_0$ (i.e. $a^3 c_0 = 0.05$ in **Figure 3b**), the monotonous decrease of $\kappa_m^{-1} / \kappa^{-1}$ with $|n_0|$ as achieved at
 369 lower $a^3 c_0$ is replaced by a non-monotonous dependence with the apparition of a minimum at sufficiently
 370 low $|n_0|$. This minimum is the signature of a significant contribution of the excluded volume of the ions as
 371 they become increasingly packed within the shell to neutralize the structural shell charges. It is even so
 372 that for extreme values of $a^3 c_0$, the underlying increasing branch of $\kappa_m^{-1} / \kappa^{-1}$ with $|n_0|$ dominates the
 373 overall dependence of $\kappa_m^{-1} / \kappa^{-1}$ on $|n_0|$ with the ensuing disappearance of the minimum invoked
 374 previously (cf. case $a^3 c_0 = 0.2$ in **Figure 3b**). In other words, the larger is $a^3 c_0$ (or ν) and/or $|n_0|$, the more
 375 the steric effects mediated by ions size dominate the impacts of the aforementioned ' y_D -effect' on
 376 $\kappa_m^{-1} / \kappa^{-1}$ which – if solely considered – would translate into a continuous decrease of $\kappa_m^{-1} / \kappa^{-1}$ with
 377 increasing $|n_0|$ or, equivalently, $|y_D|$. A noticeable consequence of such marked ions-related steric effects
 378 is that they may lead to a ratio $\kappa_m^{-1} / \kappa^{-1}$ which exceeds unity, a finding that cannot be predicted on the
 379 basis of point-like -based derivations [62] (Eq. (5)): steric effects then severely limit the screening power
 380 of the ions in moderate to highly charged shell layers as compared to that at the electrolyte side of the
 381 shell/solution interface. For extreme values of $|n_0|$, the resulting 'abrupt' increase in $\kappa_m^{-1} / \kappa^{-1}$ is
 382 materialized by a vertical asymptote $\kappa_m^{-1} \rightarrow \infty$, and this asymptote identifies with the $|n_0|$ -boundary above
 383 which the Donnan potential y_D is no longer defined (cf. **Figure 3a**) due to severely constrained
 384 accumulation of ions within the shell. Last, for any fixed values of n_0 , $\kappa_m^{-1} / \kappa^{-1}$ increases with the ion size
 385 $a^3 c_0$, and it remains strictly superior to $\kappa_{m,ref}^{-1} / \kappa^{-1}$ (Eqs. (5) and (10)), as expected.

386 **Figures 3c,d** illustrate how the valence z of the counterions and coions of given volume fraction $a^3 c_0$
 387 affect the dependence of $y_D / y_D|_{\nu=0}$ (**Figure 3c**) and $\kappa_m^{-1} / \kappa^{-1}$ (**Figure 3d**) on $|n_0|$. In addition to the ion

388 size effect captured by **Figure 3a** and leading to increasing values of $y_D / y_D|_{v=0}$ with $|n_0|$, **Figure 3c** shows
 389 that $y_D / y_D|_{v=0}$ significantly increases with z at fixed $|n_0|$. In turn, the positioning of the vertical
 390 asymptotes $n_0 = n_0^*$ defining the existence domain of the Donnan potential (i.e. $|n_0| < |n_0^*|$), is shifted to
 391 lower values of n_0^* in agreement with $|n_0^*| = 1 / (vz) = 1 / (2a^3c_0z)$ applicable to symmetrical electrolytes.
 392 **Figure 3d** shows that at low $|n_0|$ and $v \ll 1$ ($a^3c_0 = 0.02$ is adopted in **Figures 3c,d**), $\kappa_m^{-1} / \kappa^{-1}$ decreases
 393 with $|n_0|$ and correctly follows the predictions by Eq. (5) (cf. dashed curves in **Figure 3d**), in line with the
 394 manifestation of the ' y_D -effect' defined from the discussion of **Figure 3b**. This decrease of $\kappa_m^{-1} / \kappa^{-1}$ gets
 395 stronger with increasing z as the asymmetry of the potential distribution at the shell/solution interface
 396 is more pronounced for multivalent electrolytes, a feature that also emerges from Eq. (5) (cf. the argument
 397 of the hyperbolic cosine function in Eq. (5)). For larger $|n_0|$, and similarly to **Figure 3b**, the excluded volume
 398 of the ions lead to a minimum in the curves $\kappa_m^{-1} / \kappa^{-1}$ versus n_0 , and this minimum marks the onset of
 399 establishment of the vertical asymptote for $\kappa_m^{-1} / \kappa^{-1}$. In further agreement with **Figure 3c**, the threshold
 400 value $|n_0^*|$ defining this asymptote decreases significantly as ion valence gets higher: qualitatively, z acts
 401 on $y_D / y_D|_{v=0}$ and $\kappa_m^{-1} / \kappa^{-1}$ in a way comparable to that discussed for the ion volume a^3c_0 in **Figures 3a,b**.
 402 In the scenario treated by **Figures 3c,d**, the increase of the individual charge carried by the ions thus drives
 403 a higher accumulation of the counterions in shells defined by low charge density $|n_0|$, which tends to
 404 increase the screening of the potential within the shell and to decrease $\kappa_m^{-1} / \kappa^{-1}$ (' y_D -effect'). At larger
 405 $|n_0|$, ion steric effects become important and ultimately generate the vertical asymptote $\kappa_m^{-1} \rightarrow \infty$, which
 406 reflects a significant decrease in the screening of the electrolyte ions in the shell. The valence z thus
 407 effectively increases the excluded volume of the ions which is given by a^3c_0z [60]. In turn, steric exclusion
 408 of counterions from the shell is enhanced for multivalent electrolytes, which significantly lowers the
 409 corresponding $|n_0^*|$ -boundary that defines the existence domain of y_D .

410 Overall, getting back to the condition $\kappa_m \delta \gg 1$ for establishment of a Donnan phase, an increase in
 411 size and/or valence of the ions of a given symmetrical electrolyte basically leads to an increase in the
 412 minimum layer thickness required for the potential distribution to reach a Donnan plateau value y_D
 413 (when defined) in comparison to classical point-like predictions (result valid for significantly charged

414 particle shell). This condition adds to the fulfilment of the criterion $|n_0| < 1/(vz)$ defining the existence
 415 domain of y_D (Figure 2).

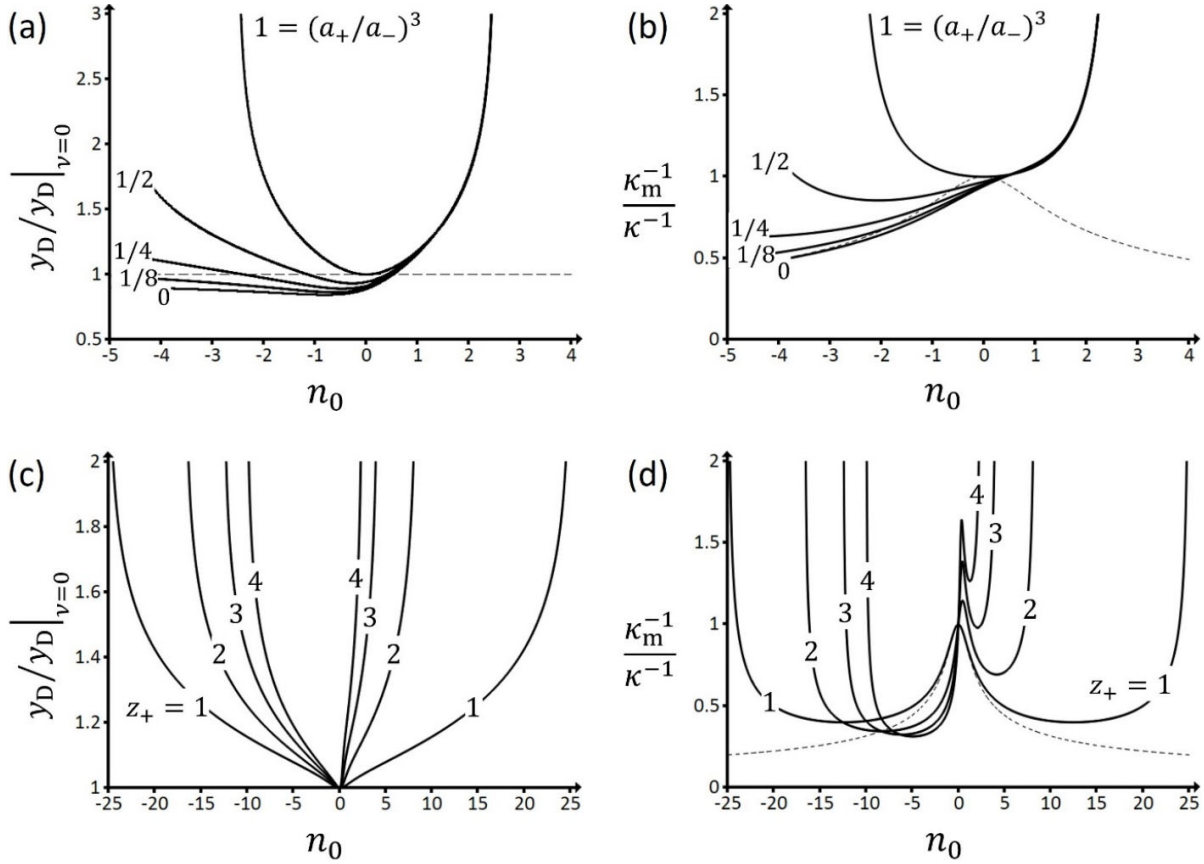


Figure 4. Donnan potential and Debye screening lengths ratios, $y_D/y_D|_{v=0}$ (a,c) and $\kappa_m^{-1}/\kappa^{-1}$ (b,d), respectively, as a function of the dimensionless structural charge density n_0 for soft surface layers in contact with asymmetrical electrolytes defined by : (a,b) $z_{+,-}=1$ and different cation/anion volume ratios $(a_+/a_-)^3$ (indicated) at fixed anion size $a_-^3 c_0 = 0.2$, and (c,d) $a_{+,-}^3 c_0 = 0.02$ and different cation valences z_+ (indicated) at fixed anion valence $z_- = 1$. Results are here given with neglecting the steric effects connected to the size of the shell charges, i.e. $a_{\text{fix}}^3 c_{\text{fix},0} \rightarrow 0$. Dashed curves in (b,d) refer to the ratio $\kappa_{\text{m,ref}}^{-1}/\kappa^{-1}$ (Eq. (5)) for $z_{+,-}=1$. The horizontal dashed line in (a) helps the reader identifying the interval of n_0 values for which $y_D < y_D|_{v=0}$, depending on the ion size ratio a_+/a_- .

416

417 For electrolytes where the cation/anion size ratio a_+/a_- differs from unity, and further considering

418 $z_{+,-}=1$ and $a_-^3 c_0 = 0.2$ (the latter condition marks a significant contribution of ions excluded volume, cf.

419 **Figures 3a,b**), **Figures 4a,b** evidence that the dependences of $y_D/y_D|_{v=0}$ and $\kappa_m^{-1}/\kappa^{-1}$ on n_0 become

420 strongly asymmetric, and the minimum reached by $y_D / y_D|_{v=0}$ (**Figure 4a**) is now shifted to higher $|n_0|$
 421 with decreasing a_+ / a_- . Starting with the case $a_+ / a_- = 1$, a decrease in the size of the cations a_+ at fixed
 422 anion size a_- generates insignificant changes in $y_D / y_D|_{v=0}$ and $\kappa_m^{-1} / \kappa^{-1}$ for $n_0 > 0$ simply because the
 423 cations then act as coions and are thus the minor ionic species within the charged shell, and even more
 424 so as n_0 gets more positive. In contrast, a decrease of a_+ / a_- at fixed a_- leads to a decrease of the
 425 excluded volume effects pertaining to the counterions for negatively charged shell layers of given n_0 (and
 426 a companion increase of their screening of the shell charge), thereby lowering both $y_D / y_D|_{v=0}$ (**Figure 4a**)
 427 and $\kappa_m^{-1} / \kappa^{-1}$ (**Figure 4b**). Remarkably, as long as $a_+ / a_- < 1$, the quantity $y_D / y_D|_{v=0}$ becomes lower than
 428 unity at sufficiently low $|n_0|$ and, within this range of $|n_0|$ values, $y_D / y_D|_{v=0}$ reaches a minimum for the
 429 reasons already invoked in **Figure 3a**. For $a_+ / a_- \rightarrow 0$ and very large $|n_0|$ in line with a complete exclusion
 430 of the coions (anions) from the negatively charged shell, the limit $y_D / y_D|_{v=0} \rightarrow 1$ is properly retrieved (not
 431 shown). As far as the ratio $\kappa_m^{-1} / \kappa^{-1}$ is concerned, it is lower than $\kappa_{m,\text{ref}}^{-1} / \kappa^{-1}$ (dashed curves in **Figure 4b**)
 432 over a range of $|n_0|$ values that expands upon lowering a_+ / a_- . In the limit $a_+ / a_- \rightarrow 0$, κ_m^{-1} correctly
 433 approaches the point-like limit $\kappa_{m,\text{ref}}^{-1}$ for $|n_0| \gg 1$ (with $n_0 < 0$) where coions are then entirely excluded
 434 from the shell layer. The above scenarios where $y_D / y_D|_{v=0} < 1$ and $\kappa_m^{-1} < \kappa_{m,\text{ref}}^{-1}$ (applicable for given ranges
 435 of $n_0 (< 0)$ and $a_+ / a_- < 1$ at fixed a_-) may appear counterintuitive as the point-like description of ions
 436 partitioning at the shell/solution interface should a priori refer to the situation where screening effects by
 437 the ions in the shell are most pronounced as their accumulation therein is not constrained by their size.
 438 However, the developments in §2.3.2 (Eq. (11)) evidenced that such screening effects are achieved not
 439 only for $a_{+,-} = 0$ but also for $a_+ = a_-$ at $|n_0| \ll 1$ recalling that the limit $\kappa_m^{-1} \rightarrow \kappa^{-1}$ is obtained under such
 440 conditions (**Figure 3b**). In turn, for ratios a_+ / a_- strictly lower than unity and at sufficiently low $|n_0|$, the
 441 screening power of the counterions in the shell is necessarily enhanced as compared to that expected on
 442 the basis of ‘point-like’ considerations, which leads to the aforementioned situations where $y_D / y_D|_{v=0} < 1$
 443 and $\kappa_m^{-1} < \kappa_{m,\text{ref}}^{-1}$. The same argument explains the inequality $\kappa_{\text{mod}}^{-1} \leq \kappa^{-1}$ given in §2.3.2.

444 In **Figures 4c,d**, we consider electrolytes where $a_+ = a_- (\neq 0)$ and we vary the value of $z_+ (\geq z_-)$ at fixed
 445 $z_- = 1$. While displaying – for a given z_+ – a dependence of $y_D / y_D|_{v=0}$ on $|n_0|$ that is qualitatively similar
 446 to that commented in **Figure 3c**, **Figure 4c** further shows that $y_D / y_D|_{v=0}$ increases with z_+ at fixed $|n_0|$.

447 For $n_0 < 0$ (range where cations are the counterions), the magnitude of this increase in $y_D / y_D|_{v=0}$ is
 448 significantly smaller than that observed for $n_0 > 0$, which generates a marked asymmetry of the plots
 449 $y_D / y_D|_{v=0}$ versus n_0 with respect to the line of equation $n_0 = 0$. This finding relates to the respective
 450 dependence of the excluded volumes of cations and anions defined by $a^3 c_+^\infty = a^3 c_0 z_-$ and $a^3 c_-^\infty = a^3 c_0 z_+$,
 451 respectively. In turn, increasing z_+ at fixed $a^3 c_0$ and fixed z_- will most significantly reduce the screening
 452 of the shell charge by electrolyte ions for $n_0 > 0$ where anions are the counterions. This is materialized by
 453 an increase of $y_D / y_D|_{v=0}$ with z_+ at given $|n_0|$ which is steeper for $n_0 > 0$ than it is for $n_0 < 0$, with a
 454 resulting reduction of the range of n_0 values where y_D is defined.

455 **Figure 4d** provides the ratio $\kappa_m^{-1} / \kappa^{-1}$ as a function of n_0 under the conditions examined in **Figure 4c**.
 456 For a negatively charged shell, starting from the reference situation $z_+ = z_- = 1$ already discussed in **Figure**
 457 **3d**, the minimum reached by $\kappa_m^{-1} / \kappa^{-1}$ decreases here with increasing z_+ and is shifted to decreasing
 458 values of $|n_0|$. This change in the position of the minima with varying z_+ is consistent with the positioning
 459 of the vertical asymptotes defining the frontier of the n_0 -domain where y_D exists in **Figure 4c**. The origin
 460 of the decrease of the minimum in $\kappa_m^{-1} / \kappa^{-1}$ with increasing z_+ is similar to that predicted by Eq. (5) for
 461 increasing values of the valence of symmetrical electrolytes. For $n_0 > 0$, the vertical asymptotes are again
 462 in agreement with the results provided in **Figure 4c**, and so is the positioning of the minima in $\kappa_m^{-1} / \kappa^{-1}$
 463 with increasing z_+ . The new feature is the increase of $\kappa_m^{-1} / \kappa^{-1}$ with increasing n_0 from 0 to $n_0 \sim 0.5$, and
 464 this increase is more important as z_+ gets higher. Then, similarly to the cases tackled in **Figure 3d**, $\kappa_m^{-1} / \kappa^{-1}$
 465 decreases at larger n_0 , and reaches a minimum that precedes the asymptotic behaviour at $n_0 = n_0^*$. The
 466 initial increase of $\kappa_m^{-1} / \kappa^{-1}$ at low (positive) n_0 stems from anions-excluded volume effects that are
 467 enhanced with increasing z_+ at fixed $a^3 c_0$ and z_- , as argued previously (cf. **Figure 4c**). For moderate values
 468 of n_0 , the decrease in $\kappa_m^{-1} / \kappa^{-1}$ with n_0 (or y_D) is explained by a stronger asymmetry of the potential
 469 profiles at both sides of the shell/solution interface (the ' y_D -effect' captured by Eq. (5)). For extreme
 470 values of n_0 , the steric limit of anions accumulation in the shell is approached, which gives rise to the
 471 increase of $\kappa_m^{-1} / \kappa^{-1}$ and to the associated apparition of the vertical asymptote.

472 As a last remark on **Figure 4** and following the discussion in §2.3.2 (cf. Eq. (11)), for electrolytes where
 473 cations and anions differ in size, κ_{mod}^{-1} may appear as a better descriptor (compared to κ^{-1}) of the electrical

474 double layer thickness operative at the electrolyte side of the shell/electrolyte interface. Therefore, we
 475 provide in **Figure S1** (Supplementary Material) the ratio $\kappa_m^{-1} / \kappa_{\text{mod}}^{-1}$ for some of the conditions examined in
 476 **Figures 4b,d**. Basically, there are no new features emerging from **Figure S1** while quantitative differences
 477 between data in **Figure S1** and **Figure 4b,d** are simply explained by the very dependence of κ_{mod}^{-1} on cations
 478 and anions sizes (cf. Eq. (11)). The reader is referred to **SM** for further details. For the sake of
 479 completeness, we mention that varying the size ratio $a_- / a_+ (< 1)$ at fixed a_+ for $z_- > z_+$ and $z_+ = 1$
 480 generate evolutions of $y_D / y_D|_{v=0}$ and $\kappa_m^{-1} / \kappa^{-1}$ with n_0 that are the symmetric (with respect to the axis
 481 $n_0 = 0$) of those displayed in **Figure 4**, because roles of cations and anions are then interchanged.

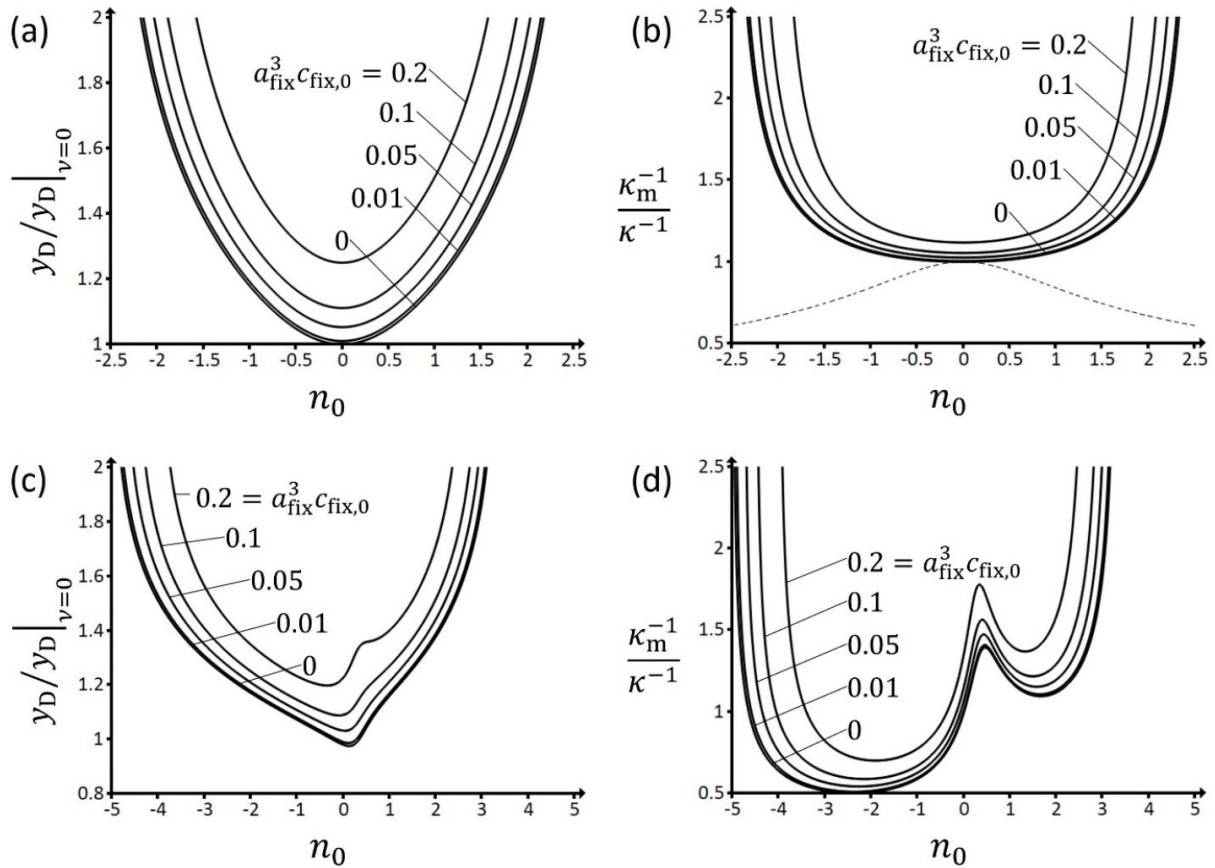


Figure 5. Donnan potential and Debye screening lengths ratios, $y_D / y_D|_{v=0}$ (**a,c**) and $\kappa_m^{-1} / \kappa^{-1}$ (**b,d**), respectively, as a function of the dimensionless structural charge density n_0 for soft surface layers whose charges are defined by a dimensionless excluded volume $a_{\text{fix}}^3 c_{\text{fix},0}$ (indicated), and which are in contact with: (**a,b**) a symmetrical electrolyte defined by $a^3 c_0 = 0.2$ and $z = 1$, and (**c,d**) an asymmetrical

electrolyte defined by $z_- = 1$, $z_+ = 3$, $a_+^3 c_0 = 0.05$ and $a_-^3 c_0 = 0.025$. Dashed curve in **(b)** refers to the ratio $\kappa_{m,\text{ref}}^{-1} / \kappa^{-1}$ (Eq. (5)) for $z_{+,-} = 1$.

482

483 Finally, **Figure 5** illustrates the impact of the excluded volume of the shell charges, $a_{\text{fix}}^3 c_{\text{fix},0}$, on
484 $y_D / y_D|_{v=0}$ and $\kappa_m^{-1} / \kappa^{-1}$ for both symmetrical (**Figures 5a,b**) and asymmetrical (**Figures 5c,d**) electrolytes
485 in terms of cations/anions size and valence. For all treated cases, the shapes of the curves $y_D / y_D|_{v=0}$ and
486 $\kappa_m^{-1} / \kappa^{-1}$ versus n_0 conform to those discussed in **Figure 3** and **Figure 4** for $a_{\text{fix}}^3 c_{\text{fix},0} \rightarrow 0$ (symmetrical and
487 unsymmetrical electrolyte conditions, respectively), and **Figure 5** shows that an increase in $a_{\text{fix}}^3 c_{\text{fix},0}$ leads
488 to a shift of both $y_D / y_D|_{v=0}$ and $\kappa_m^{-1} / \kappa^{-1}$ to larger values over the whole range of n_0 conditions. Indeed,
489 larger volume fractions of structural charges in the shell necessarily imply lower densities of electrolyte
490 ions therein (regardless of their valence and size), which reduces the screening of the shell charges by the
491 ions accumulated therein. In turn, the account of a finite $a_{\text{fix}}^3 c_{\text{fix},0}$ systematically results in a narrower n_0 -
492 domain where a Donnan potential can be established in the shell, in agreement with e.g. the equation of
493 the boundary $|n_0^*| = (1 - a_{\text{fix}}^3 c_{\text{fix},0}) / (vz)$ applicable to symmetrical electrolytes (cf. **Figure 2** and Eq. (7)).

494

495 **4. Conclusions.**

496 In this work, we discuss the conditional existence of a Donnan potential within a charged
497 polyelectrolytic particle shell with explicit account of steric effects mediated by the size and valence of
498 the electrolyte ions and the size of the structural charges carried by the shell. Based on recent corrections
499 of mean-field Poisson-Boltzmann theory for steric effects [60], we develop a formalism that addresses
500 both the existence and magnitude of the Donnan potential in the shell over a large spectrum of electrolyte
501 conditions in terms of (a)symmetry of counterions/coions size and/or valence. The results evidence that
502 a Donnan potential is achieved in a given shell layer pending the fulfilment of two criteria: (i) the
503 accumulation of counterions in the shell leading to neutralization of the structural charges therein is not
504 limited by steric effects, and (ii) the layer thickness is sufficient for the establishment of a zero-electric
505 field region (the Donnan phase) in the particle shell. The first criterion (i) is defined from systematic
506 evaluation of the dependence of the Donnan potential on a dimensionless shell charge density involving
507 solution ionic strength, for various molecular properties of the electrolyte and shell layer. The method
508 then identifies the conditions where shell charge neutralization is physically possible and those where it
509 is not. The second criterion (ii) involves the characteristic screening Debye length operative in the shell

510 layer that we formulate explicitly as a function of the excluded volumes of the electrolyte ions and shell
511 charges. In turn, a zero-electric field is reached in the shell provided that the shell thickness well exceeds
512 this intra-shell screening Debye length. Additional comparison of criteria (i) and (ii) to outcomes where
513 ions and shell charges are assimilated to immaterial points makes it further possible to identify and explain
514 the situations where the Donnan potential and the magnitude of electrolyte screening is over- or under-
515 estimated by classical mean field electrostatic theory for soft surfaces. To summarize, for symmetrical
516 electrolytes (cations/anions featuring similar size *and* valence), the excluded volumes of the counterions
517 in the shell lead to a decrease of screening of the shell charges, an increase in Donnan potential (in
518 absolute value) and a reduction of the interval of shell density values for which a Donnan phase is
519 established. These effects, depending on the magnitude of the Donnan potential and molecular
520 descriptors of the electrolyte, may associate with a marked asymmetry of the potential distribution at the
521 shell/solution interface. For asymmetrical electrolytes, the differentiated contributions of the excluded
522 volumes pertaining to the counterions and coions may lead to situations where the shell charge screening
523 exceeds the one predicted by point-like electrostatic theory.

524 Given the importance of Donnan theory for the electrostatics and electrokinetics of soft particles and
525 soft macroscopic surfaces [62-64], the current work may be valuable to address the domain of validity of
526 this theory, especially for biological particles under high salt concentration conditions where steric effects
527 can be significant. In another context, binding of metal ions and protons to particulate organic matter is
528 commonly evaluated by equilibrium Non-Ideal Competitive Adsorption (NICA)-Donnan model [65]. While
529 the limits of that model have been identified and alternatives proposed [66,67], the results reported in
530 this work allow a refined identification of the conditions underlying the applicability of the Donnan
531 electrostatic framework depending on particle size and charge, solution ionic strength, size and valence
532 of the background electrolyte ions. Future follow-up of this work includes the extension of the here-
533 reported formalism to complex electrolyte mixtures – as required for the analysis of particle electrostatics
534 in natural waters – so as to decipher the impacts of asymmetries in size and valence of the different types
535 of involved coions and counterions on the overall ion-accumulation capacity of the particle soft
536 component. Finally, it is believed that the formalism can offer a valuable mechanistic framework to
537 analyse the partitioning of ions in hydrogels depending on outer electrolyte composition, which is
538 required in e.g. polymer-based applications for the removal of contaminants in water and wastewater
539 treatment [68].

540

541 **CRedit authorship contribution statement.**

542 **Nicolas Lesniewska:** Methodology, Software, Formal analysis, Validation, Investigation, Writing - original
543 draft. **Audrey Beaussart:** Investigation, Writing - review & editing, Supervision. **Jérôme F.L. Duval:**
544 Conceptualization, Methodology, Software, Formal analysis, Investigation, Writing - review & editing,
545 Supervision.

546
547 **Declaration of Competing Interest.** The authors declare that they have no known competing financial
548 interests or personal relationships that could have appeared to influence the work reported in this paper.

549
550 **Supplementary material.** Supplementary data to this article can be found online at <https://doi.org/XXX>.

551

552 **Glossary of symbols.**

553 **Latin symbols**

554 a_+ , a_- , a_{fix} effective radii of cations, anions and shell charges (m), respectively

555 $c_+(r)$, $c_-(r)$ number densities of cations and anions (m^{-3}) at position r , respectively, with corresponding

556 bulk solution values defined by $c_+^\infty = c_0 z_-$ and $c_-^\infty = c_0 z_+$

557 $c_{\text{fix}}(r)$ number density of shell charges at position r , defined by $c_{\text{fix}}(r) = |\rho_{\text{fix}}(r)| / (Ze)$

558 $c_{\text{fix},0}$ defined by $c_{\text{fix},0} = c_{\text{fix}}(r = r_c)$

559 I solution ionic strength (mol m^{-3})

560 n_0 dimensionless density of structural charges in the shell

561 n_0^* frontier of the n_0 -domain for which a Donnan potential is defined within a shell layer

562 $n_+(r)$, $n_-(r)$ dimensionless densities of cations and anions at position r , respectively

563 r radial coordinate (m)

564 r_c hard particle core radius (m)

565 r_p soft particle radius (m), with $r_p = r_c + \delta$

566 X dimensionless space variable defined by $X = \kappa(r - r_c)$

567 $y(r)$ dimensionless potential at position r

568 y_D dimensionless Donnan potential

569 y_0 dimensionless potential at the position $r = r_p$ (cf. Figure 1)

570 z_+ , z_- , Z unsigned valences of cations, anions and shell charges respectively

571 **Greek symbols**

572 δ soft layer thickness (m)

573 ϵ_0 dielectric permittivity of vacuum (F m^{-1})

574 ϵ_s relative dielectric permittivity of the solvent (water)

575 $1/\kappa$ Debye length in solution, without account of steric effects (m)

576 $1/\kappa_m$ Debye length operative in the shell region, with account of steric effects (m) (Eqs. (9)-(10))

577 $1/\kappa_{m,\text{ref}}$ Debye length operative in the shell region, without account of steric effects (m) (Eq. (5))

578 $1/\kappa_{\text{mod}}$ Debye length in solution corrected for ion steric effects (m) (Eq. (11))

579 ν measure of the nondiluteness of the electrolyte, $\nu = a_+^3 c_+^\infty + a_-^3 c_-^\infty$

580 ρ_0 density of structural charges homogeneously distributed within the shell (C m^{-3})

581 $\rho_{\text{fix}}(r)$ density of structural charges at position r (C m^{-3}), as defined by Eq. (1)

582 $\psi(r)$ electrostatic potential at position r (V)

583 **References.**

584 [1] J. Lyklema, Fundamentals of interface and colloid science. Volume IV: Particulate colloids, Chapter 3
585 Academic Press, London, 2005.

586 [2] C.Y. Son, Z.-G. Wang, Image-charge effects on ion adsorption near aqueous interfaces, Proc. Natl. Acad.
587 Sci. U.S.A 118 (2021) e2020615118.

588 [3] H. Ohshima, Theory of electrostatics and electrokinetics of soft particles, Sci. Technol. Adv. Mater.
589 (2009) 10, 063001.

590 [4] C.G. Lopez, T. Lohmeier, J.E. Wong, W. Richtering, Electrostatic expansion of polyelectrolyte microgels:
591 effect of solvent quality and added salt, J. Colloid Interface Sci. 558 (2020) 200-210.

592 [5] N. Tamura, S. Itoh, M. Nishimura, Existence of two types of electrostatic interaction in reactions
593 catalyzed by Ferredoxin-NADP oxidoreductase, Plant and Cell Physiology 25 (1984) 589-599.

594 [6] Y. Ma, K. Poole, J. Goyette, K. Gaus, Introducing membrane charge and membrane potential to T cell
595 signaling, Front. Immunol. 8 (2017) 1513.

596 [7] O. Alegun, A. Pandeya, J. Cui, I. Ojo, Y. Wei, Donnan potential across the outer membrane of Gram-
597 negative bacteria and its effect on the permeability of antibiotics, Antibiotics 10 (2021) 701.

598 [8] G. Laucirica, M.E. Toimil-Molares, C. Trautmann, W. Marmisollé, O. Azzaroni, Nanofluidic osmotic
599 power generators - advanced nanoporous membranes and nanochannels for blue energy harvesting.
600 Chem. Sci. 12 (2021) 12874-12910.

601 [9] P. Debye, H. Hückel, The theory of electrolytes. I. The lowering of the freezing point and related
602 occurrences, Physik. Z. 24 (1923) 185.

603 [10] A.R. Denton, Poisson-Boltzmann theory of charged colloids: limits of the cell model for salty
604 suspensions, J. Phys.: Condens. Matter 22 (2010) 364108.

605 [11] S. Levine, G.M. Bell, Theory of a modified Poisson-Boltzmann equation. I. the volume effect of
606 hydrated ions, J. Phys. Chem. 64 (1960) 1188-1195.

607 [12] C.W. Outhwaite, A modified Poisson-Boltzmann equation in electric double layer theory for a
608 primitive model electrolyte with size-asymmetric ions, J. Chem. Phys. 84 (1986) 3461.

609 [13] J.J. Lopez-García, M.J. Aranda-Rascon, J. Horno, Electrical double layer around a spherical colloid
610 particle: The excluded volume effect, J. Colloid Interface Sci. 316 (2007) 196-201.

611 [14] A. Abrashkin, D. Andelman, H. Orland, Dipolar Poisson-Boltzmann equation: ions and dipoles close to
612 charge interfaces, Phys. Rev. Lett. 99 (2007) 077801.

613 [15] P. Koehl, H. Orland, M. Delarue, Adapting Poisson-Boltzmann to the self-consistent mean field theory:
614 application to protein side-chain modelling, J. Chem. Phys. 135 (2011) 055104.

615 [16] D. Ben-Yaakov, D. Andelman, R. Podgornik, D. Harries, Ion-specific hydration effects: Extending the
616 Poisson-Boltzmann theory, Curr. Opin. Colloid Interface Sci. 16 (2011) 542-550.

617 [17] P.H.R. Alijo, F.W. Tavares, E.C. Biscaia Jr., Double layer interaction between charged parallel plates
618 using a modified Poisson-Boltzmann equation to include size effects and ion specificity, Colloids Surf. A
619 Physicochem. Eng. Asp. 412 (2012) 29-35.

620 [18] J.J. Lopez-García, J. Horno, C. Grosse, Influence of the finite size and effective permittivity of ions on
621 the equilibrium double layer around colloidal particles in aqueous electrolyte solution, J. Colloid Interface
622 Sci. 428 (2014) 308-315.

623 [19] Yu. A. Budkov, A.L. Kolesnikov, M.G. Kiselev, A modified Poisson-Boltzmann theory: effects of co-
624 solvent polarizability, EPL 111 (2015) 28002.

625 [20] R. M. Adar, T. Markovich, D. Andelman, Bjerrum pairs in ionic solutions: A Poisson-Boltzmann
626 approach, *J. Chem. Phys.* 146 (2017) 194904.
627 [21] A. Gupta, H.A. Stone, Electrical double layers: effects of asymmetry in electrolyte valence on steric
628 effects, dielectric decrement, and ion-ion correlations, *Langmuir* 34 (2018) 11971-11985.
629 [22] H. Sugioka, Expanded ion-conserving Poisson-Boltzmann theory at extremely-high voltages, *Colloids*
630 *Surf. A Physicochem. Eng. Asp.* 630 (2021) 127667.
631 [23] J.-F. Dufrêche, V. Marry, O. Bernard, P. Turq, Models for electrokinetic phenomena in
632 montmorillonite, *Colloids Surf. A Physicochem. Eng. Asp.* 195 (2001) 171-180.
633 [24] G. Le Breton, L. Joly, Molecular modeling of aqueous electrolytes at interfaces: Effects of long-range
634 dispersion forces and of ionic charge rescaling, *J. Chem. Phys.* 152 (2020) 241102.
635 [25] X. Shen, I.C. Bourg, Molecular dynamics simulations of the colloidal interaction between smectite clay
636 nanoparticles in liquid water, *J. Colloid Interface Sci.* 584 (2021) 610-621.
637 [26] H. Zhang, J. Zheng, C. Lin, S. Yuan, Molecular dynamics study on adsorption and desorption of
638 lysozyme above polymer antifouling membranes, *Colloids Surf. A Physicochem. Eng. Asp.* 649 (2022)
639 129466.
640 [27] D.K. Deka, S. Pati, Electrocoalescence dynamics of two unequal-sized droplets, *Colloids Surf. A*
641 *Physicochem. Eng. Asp.* 664 (2023) 131152.
642 [28] H.-Y. Zhang, R.J. Hill, Lipopolymer electrophoresis in supported bilayer membranes, *Soft Matter*, 6
643 (2010) 5625-5635.
644 [29] H. Ohshima, Electrophoresis of soft particles, *Adv. Coll. Interface Sci.* 62 (1995) 189-235.
645 [30] J.F.L. Duval, C. Werner, R. Zimmermann, Electrokinetics of soft polymeric interphases with layered
646 distribution of anionic and cationic charges, *Curr. Opin. Colloid Interface Sci.* 24 (2016) 1-12.
647 [31] J.F.L. Duval, F. Gaboriaud, Progress in electrohydrodynamics of soft microbial particle interphases.
648 *Curr. Opin. Colloid Interface Sci.* 15 (2010) 184-195.
649 [32] P.P. Gopmandal, J.F.L. Duval, Electrostatics and electrophoresis of engineered nanoparticles and
650 particulate environmental contaminants: beyond zeta potential-based formulation, *Curr. Opin. Colloid*
651 *Interface Sci.* 60 (2022) 101605.
652 [33] G. Bonacucina, M. Cespi, M. Misici-Falzi, G.F. Palmieri, Colloidal soft matter as drug delivery system,
653 *J. Pharm Sci.* 98 (2009) 1-42.
654 [34] D. Jiang, X. Song, H. Zhang, M. Yuan, Removal of organic pollutants with polylactic acid-based
655 nanofiber composites, *Polymers* 14 (2022) 4622.
656 [35] X. Xu, N. Bizmark, K.S.S. Christie, S.S. Datta, Z.J. Ren, R. D. Priestley, Thermoresponsive polymers for
657 water treatment and collection, *Macromolecules* 55 (2022) 1894-1909.
658 [36] J. Bernal-Bayard, J. Thiebaud, M. Brossaud, A. Beaussart, C. Caillet, Y. Waldvogel, L. Travier, S. Létoffé,
659 T. Fontaine, B. Rokbi, P. Talaga, C. Beloin, N. Mistretta, J.F.L. Duval, J.M. Ghigo, Bacterial capsular
660 polysaccharides with antibiofilm activity share common biophysical and electrokinetic properties. *Nat.*
661 *comm.* 14 (2023) 2553.
662 [37] R. Zimmermann, S.S. Dukhin, C. Werner, J.F.L. Duval, On the use of electrokinetics for unraveling
663 charging and structure of soft planar polymer films. *Curr. Opin. Colloid Interface Sci.* 18 (2013) 83-92.
664 [38] J.F.L. Duval, D. Küttner, C. Werner, R. Zimmermann, Electrohydrodynamics of soft polyelectrolyte
665 multilayers: point of zero-streaming current, *Langmuir* 27 (2011) 10739-10752.
666 [39] R.J. Hill, D.A. Saville, W.B. Russel, Electrophoresis of spherical polymer-coated colloidal particles, *J.*
667 *Colloid Interface Sci.* 258 (2003) 56-74.
668 [40] J.J. Lopez-Garcia, C. Grosse, J.J. Horno, Numerical study of colloidal suspensions of soft spherical
669 particles using the network method: 1. DC electrophoretic mobility, *J. Colloid Interface Sci.* 265 (2003)
670 327-340.

671 [41] J.F.L. Duval, J. Merlin, J., P.A.L. Narayana, Electrostatic interactions between diffuse soft multi-layered
672 (bio)particles: beyond Debye-Hückel approximation and Deryagin formulation, *Phys. Chem. Chem. Phys.*
673 13 (2011) 1037-1053.

674 [42] H. Ohshima, Electrostatic interaction between soft particles, *J. Colloid Interface Sci.* 328 (2008) 3-9.

675 [43] H. Ohshima, Electrostatic interaction between two interpenetrating soft particles, *Colloids Surf. A*
676 *Physicochem. Eng. Asp.* 460 (2014) 448-453.

677 [44] J.F.L. Duval, H. Ohshima, Electrophoresis of diffuse soft particles, *Langmuir* 22 (2006) 3533-3546.

678 [45] H. Ohshima, S. Ohki, Donnan potential and surface potential of a charged membrane, *Biophys. J.* 47
679 (1985) 673-678.

680 [46] A. Mauro, Space charge regions in fixed charge membranes and the associated property of
681 capacitance, *Biophys. J.* 2 (1962) 179-198.

682 [47] J.F.L. Duval, H.P. van Leeuwen, Electrokinetics of diffuse soft interfaces. I. Limit of low Donnan
683 potentials, *Langmuir* 20 (2004) 10324-10336.

684 [48] J.F.L. Duval, Electrokinetics of diffuse soft interfaces. II. Analysis based on the nonlinear Poisson-
685 Boltzmann equation, *Langmuir* 21 (2005) 3247-3258.

686 [49] J.T. Davies, E.K. Rideal. 1961. *Interfacial Phenomena*. Academic Press, Inc., New York and London. 75-
687 84.

688 [50] S. Ohki, Rectification by a double membrane, *J. Phys. Soc. Jpn.* 20 (1965) 1674-1685.

689 [51] P.A. Gokturk, R. Sujanani, J. Qian, Y. Wang, L.E. Katz, B.D. Freeman, E.J. Crumlin, The Donnan potential
690 revealed, *Nat. comm.* 13 (2022) 5880.

691 [52] T.A. Davis, L.P. Yezek, J.P. Pinheiro, H.P. van Leeuwen, Measurement of Donnan potentials in gels by
692 in situ microelectrode voltammetry, *J. Electroanal. Chem.* 584 (2005) 100-109.

693 [53] C. Pagnout, A. Razafitianamaharavo, B. Sohm, C. Caillet, A. Beaussart, E. Delatour, I. Bihannic, M.
694 Offroy, M., J.F.L. Duval, Osmotic stress and vesiculation as key mechanisms controlling bacterial sensitivity
695 and resistance to TiO₂ nanoparticles, *Commun. Biol.* 4 (2021) 678.

696 [54] G. Goodwin, S. B. McMahon, The physiological function of different voltage-gated sodium channels
697 in pain. *Nat. Rev. Neurosci.* 22 (2021) 263-274.

698 [55] I. Borukhov, D. Andelman, H. Orland, Steric effects in electrolytes: a modified Poisson-Boltzmann
699 equation, *Phys. Rev. Lett.* 79 (1997) 435.

700 [56] A.G. Moreira, R.R. Netz, Strong coupling theory for counter-ion distributions, *EPL* 52 (2000) 705.

701 [57] T.-L. Horng, Review and modification of entropy modeling for steric effects in the Poisson-Boltzmann
702 equation, *Entropy* 22 (2020) 632.

703 [58] S. Chanda, S. Das, Effect of finite ion sizes in an electrostatic potential distribution for a charged soft
704 surface in contact with an electrolyte solution, *Phys. Rev. E* 89 (2014) 012307.

705 [59] P. Gopmandal, S. De, H. Ohshima, Impact of ion-steric and ion-partitioning effects on electrophoresis
706 of soft particles, *Phys. Rev. E* 102 (2020) 032601.

707 [60] N. Lesniewska, A. Beaussart, J.F.L. Duval, Electrostatics of soft (bio)interfaces: corrections of mean-
708 field Poisson-Boltzmann theory for ion size, dielectric decrement and ion-ion correlations, *J. Colloid*
709 *Interface Sci.* 642 (2023) 154-158.

710 [61] M.S. Kilic, M.Z. Bazant, Steric effects in the dynamics of electrolytes at large applied voltages. I.
711 Double-layer charging, *Phys. Rev.* 75 (2007) 021502.

712 [62] H. Ohshima, Donnan potential and surface potential of a spherical soft particle in an electrolyte
713 solution, *J. Colloid Interface Sci.* 323 (2008) 92-97.

714 [63] K. Makino, H. Ohshima, Soft particle analysis of electrokinetics of biological cells and their model
715 systems, *Sci. Technol. Adv. Mater.* 12 (2011), 023001.

716 [64] H.J. Muhren, P. van der Schoot, Electrostatic theory of the acidity of the solution in the lumina of
717 viruses and virus-like particles, *J. Phys. Chem B.* 127 (2023) 2160-2168.

- 718 [65] C.J. Milne, D.G. Kinniburgh, W.H. van Riemsdijk, E. Tipping, Generic NICA-Donnan model parameters
719 for metal-ion binding by humic substances, *Environ. Sci. Technol.* 37 (2003) 958-971.
- 720 [66] R.M. Town, H.P. van Leeuwen, J.F.L. Duval, Rigorous physicochemical framework for metal ion binding
721 by aqueous nanoparticulate humic substances: Implications for speciation modeling by the NICA-Donnan
722 and WHAM codes, *Environ. Sci. Technol.* 53 (2019) 8516-8532.
- 723 [67] J.P. Pinheiro, E. Rotureau, J.F.L. Duval, Addressing the electrostatic component of protons binding to
724 aquatic nanoparticles beyond the Non-Ideal Competitive Adsorption (NICA)-Donnan level: Theory and
725 application to analysis of proton titration data for humic matter, *J. Colloid Interface. Sci.* 583 (2021) 642-
726 651.
- 727 [68] V.V. Tran, D. Park, Y.-Ch. Lee. Hydrogel applications for adsorption of contaminants in water and
728 wastewater treatment, *Environ. Sci. Pollut. Res.* 25 (2018) 24569-24599.
- 729